Characterization of a novel passive personal fast neutron dosimeter based on a CR-39 track detector in monochromatic neutron fields via Monte Carlo simulations and experiments

Micol Bolzonella, Marco Caresana, Michele Ferrarini, Richard Babut

CHARACTERIZATION OF A NOVEL PASSIVE PERSONAL FAST NEUTRON DOSIMETER BASED ON A *CR-39* TRACK DETECTOR IN MONOCHROMATIC NEUTRON FIELDS VIA MONTE CARLO SIMULATIONS AND EXPERIMENTS

M. Bolzonella[a,*], M. Caresana[a], M. Ferrarini[b], R. Babut[c]

[a] Politecnico di Milano, Department of Energy, Via Lambruschini 4, 20156, Milan, Italy.

[b] Fondazione CNAO, Strada Privata Campeggi, Pavia, 27100, Italy.

[c] Institut de Radioprotection et de Sûreté Nucléaire (IRSN), BP 3, 13115 Saint-Paul-lez-Durance, Cedex, France.

Abstract The response in terms of personal dose equivalent of a passive fast neutron dosimeter composed by a *CR-39* detector coupled with a 1-cm-thick *PMMA* radiator is investigated in monochromatic neutron fields via simulations and experiments. In particular, the simulations were performed through the Monte Carlo *FLUKA* code (version 2011.2x.5), while the experimental fields were produced at the *IRSN-AMANDE* facility in Cadarache. The response is studied both with respect to the energy of the field and to its angle of incidence on the device. The simulated response shows a quite stationary trend in a wide energy range and also with respect to different irradiation geometries, and the agreement between simulated and experimental points individuates the simple and cheap dosimeter presented as promising for personal dosimetry applications in practical situations.

Keywords: *CR–39*, Monte Carlo simulations, *FLUKA*, Neutron fields, Passive dosimeters, Personal dosimetry

1. Introduction

Fast neutron dosimetry has become more and more relevant in the last decades due to the development of a wide range of human activities involving the presence of high-energy neutron, such as cosmic-ray neutrons in high-altitude/space activities or secondary neutrons produced in particle accelerator-based activities.

Solid state nuclear track detectors (*SSNTD*s), such as *CR-39* or *LR-115*, can be used as effective dosimeters for the fields just described, if properly calibrated **[1]**. In particular, when used for fast neutron dosimetry, *SSNTD*s are usually placed behind a proper radiator **[2]** and the signal is mainly due to charged secondaries produced by fast neutrons hitting the radiator: some of the damages to the detector polymer chains caused by such charged particles become tracks visible under a microscope after a proper chemical treatment known as *etching*.

Furthermore, such devices allow to build cheap passive dosimeters totally insensitive to the gamma background usually accompanying neutron fields.

The traditional technique for dose assessment with these dosimeters is based on simple track counting: tracks are counted and, thanks to a calibration factor, the track density is converted into the desired dosimetric quantity **[3]**,**[4]**,**[5]**,**[6]**. However, this approach turns out to be strongly field-dependent.

An alternative approach **[7]**,**[8]**,**[9]** involves the spectrometry of the linear energy transfer (*LET*) of the particles producing the signal, which is performed through the morphological analysis of the tracks: by knowing the approximate *LET* of each of these particles and some information about their direction in space, the contribution to the dosimetric quantity of interest of each particle can

* Corresponding author. Politecnico di Milano, Department of Energy, Via Lambruschini 4, 20156, Milan, Italy.
E-mail address: matteo.bolzonella@polimi.it (Matteo Bolzonella).

be derived and added to the others to obtain an estimate of this quantity. The advantage of this technique is that dosimeter working according to this principle show a quite stationary response in a variety of different neutron fields.
In this work a personal dosimeter based on this last technique is analyzed.

2. Material and methods

The dosimeter considered is composed by a *PMMA* [poly(methyl methacrylate), $(C_5O_2H_8)_n$] radiator coupled with a passive detector made of *CR-39* [poly(allyl diglycol carbonate), $(C_{12}O_7H_{18})_n$], as shown in ***Figure 1***.
The dimensions are the following: $25 \times 25 \times 10\ \text{mm}^3$ for the radiator, $25 \times 25 \times 1.5\ \text{mm}^3$ for the detector.

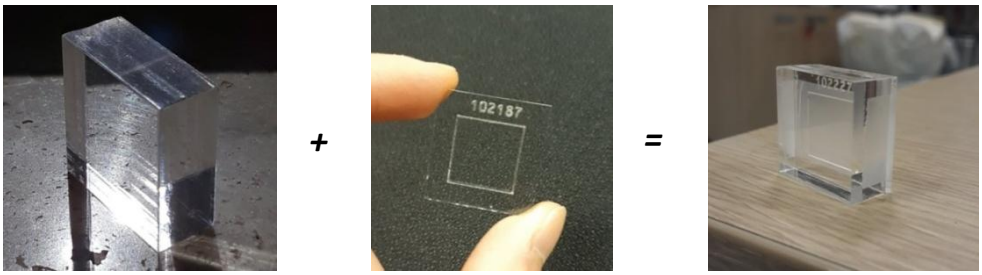

Figure 1 *– The PMMA radiator (**A**)) and PADC detector (**B**)) composing the dosimeter (**C**)).*

The working principle of the device is based on the method individuated by M. Caresana et al. **[8]**: from the morphological analysis of the tracks produced in the *CR-39* by charged particles (primaries and/or secondaries) – as exhaustively discussed in **[8]**,**[10]** – the average linear energy transfer $\overline{LET}$ along each track (limited to the portion interested by the etching process) and the impinging angle α of all particles which generated the tracks can be derived, and they can be used to obtain a good approximation of the dose equivalent in the detector sensitive volume, namely a parallelepiped the upper surface of which coincides with the *PMMA*/*CR-39* interface and with a thickness dependent on the duration of the chemical treatment **[8]**. In particular, this quantity is indicated as H_{cr} and it is given by:

$$H_{cr} = \frac{1}{\rho A} \cdot 1.602 \cdot 10^{-6} \cdot \sum_{i=1}^{n} \frac{\overline{LET}_i}{\cos \alpha_i} Q_i \qquad (1)$$

where $\overline{LET}_i$ is the mean LET along the i-th track in keV μm^{-1}, α_i denotes the particle impinging angle with respect to the *CR-39* surface normal, ρ is the *CR-39* density in g $\cdot$ cm^{-3} and Q_i is the *ICRP* quality factor. In Equation (1), the index i runs on all the n tracks and the numerical factor permits to obtain the quantity in mSv.
Due to the geometry (the sensitive volume lies below 10 mm of *PMMA*) and the material composition of the dosimeter (all its materials can be treated as tissue equivalent, *TE*, with a good approximation), H_{cr} can be successfully used as an estimate of the personal dose equivalent $H_p(10)$ when the dosimeter is placed on a solid slab phantom mimicking the operator's body.

Recalling that $H_p(10)$ depends on the specific site considered and on the irradiation geometry, it is necessary to fix a reference to evaluate the dosimeter response: in this study, this reference value is generally understood to be the dose equivalent produced by a monodirectional neutron field at *a point* 10 mm *below the center of the ICRU solid slab phantom front surface*, indicated as $H_{p,slab}\ (10;\alpha)$, associated to the most general site to estimate the dose equivalent in the human body at a depth of 1 cm due to external exposure and for which there is a wide range of information in literature **[11]**; consequently, the response is defined as:

$$R = \frac{H_{cr}}{H_{p,slab}(10;\alpha)} \tag{2}$$

The dosimeters were characterized by studying their response in monochromatic and monodirectional neutron fields via simulations using the Monte Carlo transport code *FLUKA* (version 2011.2x.5) **[12]**,**[13]** and by the means of experimental irradiations performed at the *AMANDE* facility (Accélérateur pour la Métrologie et les Applications Neutroniques en Dosimétrie Externe) **[14]**,**[15]**, an experimental facility of the *IRSN* in Cadarache, inaugurated in 2005, hosting an accelerator to produce monoenergetic neutron fields in the energy range from 2 keV to 20 MeV through selected nuclear reaction on proper target materials. Notice that the neutrons fields produced at the *AMANDE* facility, because of the kinematics of the nuclear reactions involved, are monoenergetic at a given direction (excluding the generally little contribution of scattered neutrons): for practical applications, the dosimeters are irradiated at a sufficiently high distance from the neutron producing target so that neutrons impinging on it can be approximated as monodirectional and, hence, monoenergetic.
The *ICRU* solid slab phantom was implemented for the simulations, while the *ISO* solid slab phantom was used in the experiments (both phantoms have dimensions: $30 \times 30 \times 15\ \mathrm{cm}^3$).
For the experiments four dosimeters were irradiated at a time, organized in a 2×2 matrix placed centrally onto the phantom front surface inside an area where the relative variation of the dose are $< 1\%$, while for the simulations a single dosimeter with a quadrupled surface was implemented to obtain a better counting statistics (***Figure 2***).

A) ***B)***

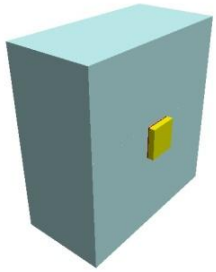

Figure 2 *- **A)** 3D rendering of the simulated setup: the PMMA radiator is shown in yellow, the CR-39 detector in red and the ICRU phantom in light blue. **B)** Experimental setup for the irradiation at the IRSN-AMANDE facility in case of normal incidence of the field, the black circle indicates an area within which the relative variations of the dose are* $< 1\%$.

As for the experiments, the response in terms of $H_{p,slab}\,(10;0°), H_{p,slab}\,(10;30°)$ and $H_{p,slab}\,(10;60°)$ was investigated considering neutron fields of energies equal to 0.565 -, 2.5 -, 5 -, 15.1 - and 17 MeV, the main features of which, including the nuclear reactions exploited to produce them, are listed in ***Table 1***.

Reaction	**Target Type**	**Thickness** ($\mu g/cm^2$)	**Incident beam energy (keV)**	**Neutron energy (keV)**	**Energy peak *FWHM* (keV)**
$Li(p,n)$	*LiF*	300.39	2311	565	36.7
$T(p,n)$	*TiT*	1960.3	3351	2500	139.0
$D(d,n)$	*TiD*	775.67	1839	5000	141.0
$T(d,n)$	*TiT*	775.67	432	15100	94.9
$T(d,n)$	*TiT*	2044.9	1378	17000	710.3

Table 1 *– Main characteristics of the neutron fields employed for the various irradiations.*

The spectra of the various fields are shown in ***Figure 3***.

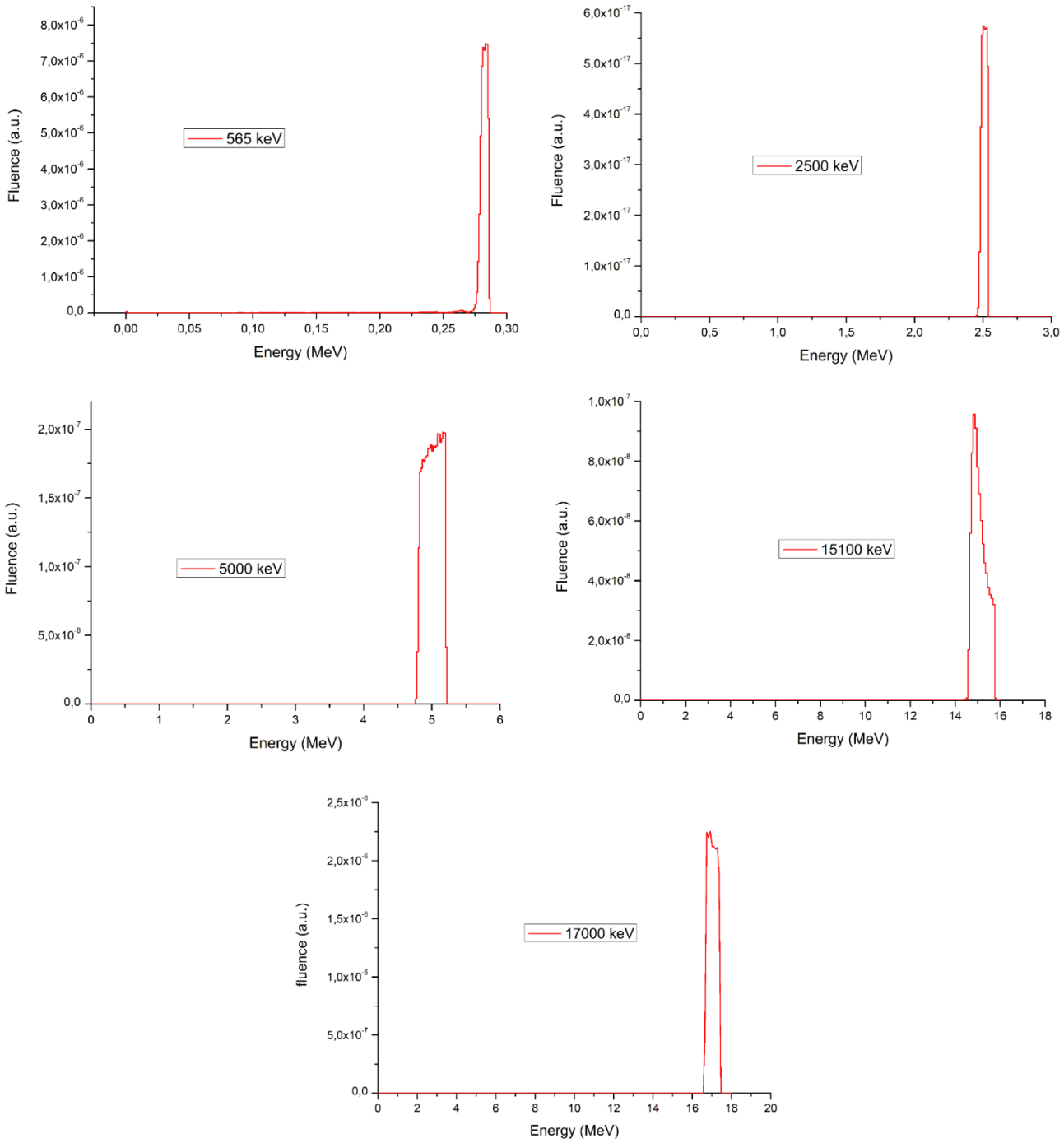

Figure 3 *– Reference spectra of the monochromatic neutron fields produced at the AMANDE facility. The various legends refer to the average energies of each spectrum.*

The phantom was placed at 75 cm from the neutron producing target and tilted by the proper angle (0°, 30° or 60°), measured between the beam extraction direction and the normal to the phantom front surface.

The reference values for the $H_{p,slab}(10;\alpha)$ of the various fields, assessed through the joint use of numerical simulations and fluence measurements, are gathered shown in ***Table 2***; note that the uncertainty corresponds to 2 standard deviations (2σ).

Neutron energy (MeV)	$H_{p,slab}(10;0°)$ (μSv)	$H_{p,slab}(10;30°)$ (μSv)	$H_{p,slab}(10;60°)$ (μSv)
0.565	3157 ± 180	3353 ± 190	3325 ± 188
2.5	3191 ± 172	3263 ± 174	3083 ± 166
5	3128 ± 170	3096 ± 168	3082 ± 168
15.1	3275 ± 222	3322 ± 226	3232 ± 110
17	3115 ± 206	3073 ± 204	3052 ± 202

Table 2 *- $H_{p,slab}(10;\alpha)$ values for the neutron fields considered.*

Fixed the neutron energy and the angle of incidence, the dosimeters were irradiated using one dosimeters matrix per irradiation. Notice that each matrix contained two dosimeters with *CR-39*s from *TASL* (Track Analysis Systems Ltd) and two with *CR-39*s from *GM Scientific Ltd*: detectors from different suppliers were employed to test them and compare their properties.

Moreover, a set of dosimeters with *TASL CR-39*s and a set of dosimeters with *GM Scientific Ltd CR-39*s were used as "background dosimeters": they were transported with the others, but they were not irradiated in order to estimate the average background signal, in terms of H_{cr}, to be associated to each *CR-39*s type (i.e., *TASL CR-39*s or *GM Scientific Ltd* ones).

Afterwards, the *CR-39* underwent a chemical etching consisting in a bath in a 6.25 mol/L aqueous solution of sodium hydroxide (*caustic soda*, $NaOH$) at 97.3 ± 0.1 °C for 70 minutes, in order to obtain an average removed layer equal to 15 μm for the undamaged material (*bulk*), defining the sensitive volume depth.

Finally, the morphological analysis of the *CR-39*s leading to the H_{cr} calculation was performed through the *Politrack*® system **[8]**, **[16]** and the experimental H_{cr} of the irradiated *CR-39*s values were obtained by subtracting the proper average background signal (depending on the *CR-39* type) from the (gross) doses returned by the *Politrack*®.

On the other hand, the simulated H_{cr} values were computed through an algorithm for the *FLUKA* code developed by our team **[17]**; the algorithm works as follows: for any particle crossing the upper or lower surface of the sensitive volume which could contribute to the signal, the corresponding $\overline{LET}$ and impinging angle α are scored and checked against the $\overline{LET}$ threshold value (10 keV/μm, according to experimental data) and the *critical angle* **[18]** value (drawn from **[19]**) that make a particle fit for producing a track and summing up the dose contributions linked to each track. The responses were then computed by Equation (2), for which the reference $H_{p,slab}(10;\alpha)$ values were obtained from *ICRP 74* **[11]**.

Simulations were performed using expanded and aligned fields at the energies of the experimental fields, except for the 15.1 MeV and the 17 MeV cases since these values lie in an energy interval which is critical: for these energies the contribution of the products of inelastic nuclear reactions on C and O is still important, but these secondaries are not explicitly transported by *FLUKA* for neutron fields of energy < 20 MeV and only for energies below about 10 MeV the contribution of the reactions aforementioned become small and it can be neglected. So, to evaluate these last two cases simulations were run at 20 MeV and at 10 MeV from which the intermediate response trend can be interpolated and compared with the experimental points.

Moreover, several additional simulations referred to characteristic neutron energies ranging from 100 keV (i.e. the nominal threshold for neutron detection using *CR-39*) to 1 GeV and considering impinging angles in the range $0° - 75°$ were performed in order to extend the study of the response to the typical energy range of interest and to the practical angles considered by *ICRP74*

[11] for the conversion coefficients from fluence to $H_{p,slab}(10;\alpha)$ (corresponding to the irradiation geometries for which $H_{p,slab}(10;\alpha)$ is a good operative approximation of the effective dose).

3. Results and discussion

The simulated and experimental points are shown in ***Figure 4***, together with their uncertainties shown in the form of error bars and equal to the sample standard deviation s; simulated responses referred to further energies were added to visualize the response trend in an ampler energy range.

Note that the reference $H_{p,slab}(10;\alpha)$ values useful to compute the response for simulations involving neutrons with energy higher than 20 MeV, but lower than 250 MeV, were obtained from Olsher et al. **[20]** since data about $H_{p,slab}(10;\alpha)$ in *ICRP74* are not available for such neutron energies.

As for neutron energies above 250 MeV, $H^*(10)$ was used in place of $H_{p,slab}(10;\alpha)$ in the response, being $H_{p,slab}(10;\alpha)$ not defined for such high energy vales, and the reference $H^*(10)$ values for these cases were drawn from the *FLUKA* `AMB74` fluence-to-$H^*(10)$ conversion coefficients set. Anyway, when the neutron energy is of the order of tens of MeV or above, $H^*(10)$ and $H_{p,slab}(10;\alpha)$ become quite similar, so that the former can be used as an operative approximation of the latter.

As it appears from ***Figure 4***, the simulated and experimental points are in agreement both as values and as trend, with maximum deviations of about $\pm 40\%$.

These deviations can be ascribed to the various assumptions included in the simulation algorithm, in particular the ones used to compute the critical angle, which is a delicate parameter and plays an important role in determining the response **[21]**, especially for near-normal incidence of the field on the device.

Comparing the various experimental points, the detection performance of the *CR-39* from *TASL* appears to be is just as good as the one of the *GM Scientific Ltd* detectors.

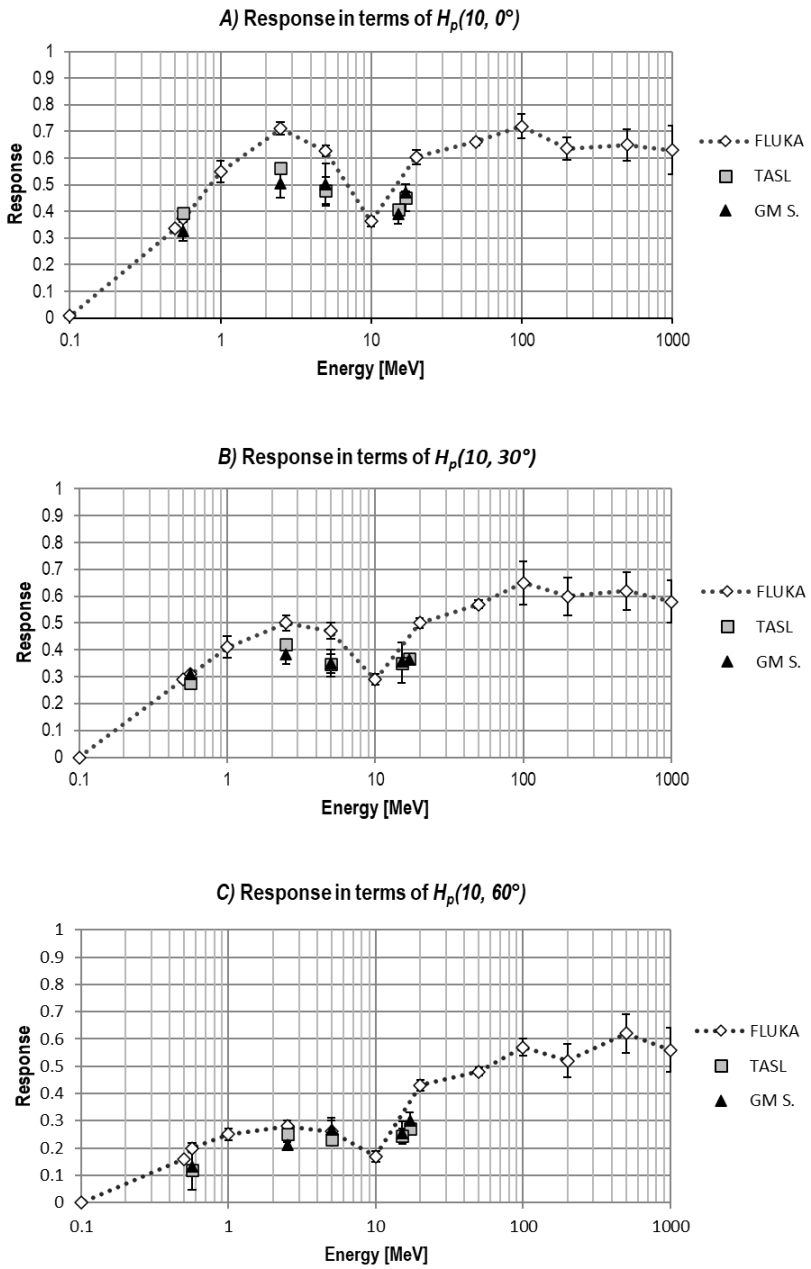

Figure 4 *– Experimental and simulated responses in terms of:* ***A)*** $H_{p,slab}$ *(10;0°);* ***B)*** $H_{p,slab}$ *(10;30°);* ***C)*** $H_{p,slab}$ *(10;60°). In the legends, "FLUKA" refers to the simulated points, "TASL" to the experimental points calculated using TASL detectors and "GM S." to the experimental points computed starting from GM Scientific Ltd detectors.*

As anticipated, simulations (in the manner described above) referred to other neutron energies (E_n) and impinging angles (α) were also performed in order to draw a more complete analysis of the dosimeter response. The results of these simulations are gathered in ***Table 3,*** some of which has already been graphically shown in ***Figure 4***.

E_n \ α	0°	15°	30°	45°	60°	75°
1 GeV [1]	0.63 ± 0.06	0.62 ± 0.05	0.58 ± 0.05	0.58 ± 0.04	0.56 ± 0.03	0.55 ± 0.05
500 MeV [1]	0.65 ± 0.04	0.63 ± 0.05	0.62 ± 0.05	0.64 ± 0.05	0.62 ± 0.06	0.59 ± 0.07
200 MeV	0.64 ± 0.09	0.62 ± 0.09	0.60 ± 0.08	0.57 ± 0.07	0.52 ± 0.08	0.49 ± 0.11
100 MeV	0.72 ± 0.06	0.70 ± 0.03	0.65 ± 0.07	0.61 ± 0.05	0.57 ± 0.07	0.50 ± 0.04
50 MeV	0.66 ± 0.04	0.63 ± 0.06	0.57 ± 0.07	0.52 ± 0.06	0.48 ± 0.06	0.46 ± 0.05
20 MeV	0.60 ± 0.05	0.57 ± 0.06	0.50 ± 0.08	0.49 ± 0.03	0.43 ± 0.03	0.40 ± 0.04
10 MeV	0.36 ± 0.01	0.35 ± 0.01	0.29 ± 0.01	0.22 ± 0.01	0.17 ± 0.01	0.13 ± 0.01
5 MeV	0.63 ± 0.03	0.62 ± 0.02	0.47 ± 0.02	0.35 ± 0.02	0.26 ± 0.02	0.22 ± 0.03
1 MeV	0.55 ± 0.02	0.52 ± 0.04	0.41 ± 0.03	0.33 ± 0.04	0.25 ± 0.04	0.29 ± 0.05
500 keV	0.34 ± 0.04	0.33 ± 0.03	0.29 ± 0.04	0.23 ± 0.04	0.16 ± 0.02	0.25 ± 0.05
100 keV	0.01 ± 0.01	0.01 ± 0.01	0.01 ± 0.00	0.01 ± 0.00	0.00 ± 0.00	0.00 ± 0.00

[1] Responses referred to $H^*(10)$.

Table 3 *– Simulated responses, each calculated as average over the results of 10 independent simulations, together with their uncertainty, intended as sample standard deviation (σ). All data are referred to expanded and aligned monochromatic neutron fields with a fluence of* 10^5 cm^{-2}*, except for the simulations with* $E_n = 100\ keV$ and $\alpha \geq 30°$ which were calculated for a neutron fluence equal to 10^6 cm^{-2} in order to achieve statistically significant values.

Figure 5 shows the 3D response trend as a function of the energy and impinging angle of the field, built interpolating data in ***Table 3***.

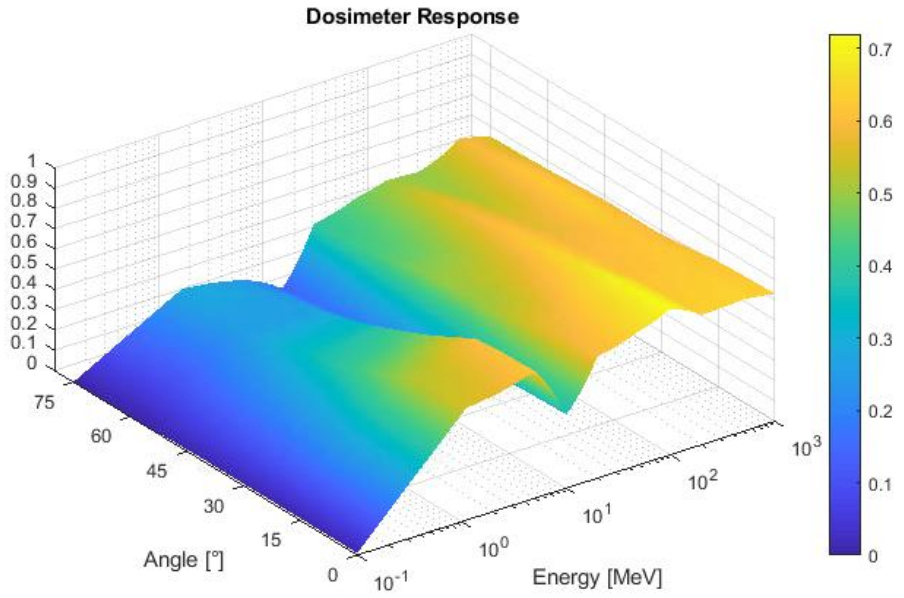

Figure 5 *– 3D graph of the dosimeter response.*

From a theoretical point of view, the response of the device in a generic neutron field is given by the weighted average of the response values referred to monochromatic fields where the weight of each component with a given energy and impinging angle is given by its contribution to the total personal dose equivalent, i.e. analytically:

$$R = \frac{\iint_{E,\alpha} R_m(E,\alpha) \cdot w_i(E,\alpha)\, \mathrm{d}\alpha \mathrm{d}E}{\iint_{E,\alpha} w_i(E,\alpha)\, \mathrm{d}\alpha \mathrm{d}E} \tag{3}$$

in which $R_m(E,\alpha)$ is the device response in monochromatic neutron fields (determinable by interpolating data in ***Table 3***) and the weights $w_i(E,\alpha)$ are given by

$$w_i(E,\alpha) = \Phi_n(E,\alpha) \cdot H_{ref,\Phi_n}(E,10,\alpha) \tag{4}$$

where $\Phi_n(E,\alpha)$ is the fluence of the field and $H_{ref,\Phi_n}(E,10,\alpha)$ indicates the conversion coefficient from fluence to the reference operational dosimetric quantity used to compute $R_m(E,\alpha)$, i.e. $H_{p,slab}(10;\alpha)$ most of the times.

In practical situations, however, the neutron spectra are not known *a priori* and no precise hypotheses can be made on the irradiation geometry so that Equation (3) cannot be applied in a rigorous way. Anyhow, as it appears from ***Figure 5***, the response trend is quite flat in a wide energetic and angular range so that, as a useful operational approach, a single average value for the response $\bar{R}$ suitable for a variety of fields can be computed reasoning on the simulated data and it can be used to obtain useful operational approximations of the personal dose equivalent simply computing:

$$H_p(10) = \frac{H_{cr}}{\bar{R}} \tag{5}$$

As a final remark, it is worthy to notice that the fall of the response for energies below 1 MeV should not concern since workplace neutron fields contain a wide range of neutron energies and neutrons with energies associated to very low response values contribute scarcely to the total dose equivalent, so that their weights in determining the average response are negligible not jeopardizing the proper working of the dosimeters in these fields.

4. Conclusions and perspectives

The simple and cheap dosimeter described in this paper shows a response quite stationary with energy, mainly due to the physical reasons explained in **§ 2**, so that it appears as a promising device for personal dosimetry in practical neutron fields. In particular, the fact that the response is quite flat in a wide energy and angular range is a remarkable result since it demonstrates that the dosimeter can work in a "*REM*-counter-like" way.

An average response could be introduced even not knowing neither the neutron field nor the irradiation geometry *a priori*, as it the typical case for practical situations, and, given the match between experimental and simulated points, it can be expected to satisfy the acceptance criteria suggested by *ISO* for dosimetry in a variety of workplace neutron fields **[22]**, also considering that the experimental response appears to be even more stationary than the simulated one.

It would certainly be very interesting to carry out further experiments to investigate the dosimeter response with respect to other angular positions and/or in other kind of fields (e.g. characterized by continuous energy spectra) as well as the lower limit of detection in terms of dose.

5. References

[1] F. Spurný, K. Turek, *Neutron Dosimetry and Solid State Nuclear Track Detectors*, Nuclear Track Detection, 1, pp. 189-197, 1977.

[2] F. Castillo, G. Espinosa, J. I. Golzarri, D. Osorio, J. Rangel, P. G. Reyes, J. J. E. Herrera, *Fast neutron dosimetry using CR-39 track detectors with polyethylene as radiator*, Radiation Measurements, 50, pp. 71-73, 2013.

[3] R. L. Fleischer, L. G. Turner, H. G. Paretzke, H. Schraube, *Personnel neutron dosimetry using particle tracks in solids: a comparison*, Health Physics, 47, pp. 521-531, 1984.

[4] R. J. Tanner, D. T. Barlett, L. G. Hager, *Operational and dosimetric characterization of etched-track neutron detectors in routine neutron radiation protection dosimetry*, Radiation Measurement, 40, pp. 549-559, 2005.

[5] G. Saint Martin, F. López, O. A. Bernaola, *Neutron dosimetry device using PADC nuclear track detectors,* Journal of Radioanalytical and Nuclear Chemistry, 287, pp. 635-638, 2011.

[6] M. R. Deevband, P. Abdolmaleki, M. R. Kardan, H. R. Khosravi, M. Taheri, F. Nazeri, N. Ahmadi, *Experimental and Monte Carlo studies on the response of CR-39 detectors to Am-Be neutron spectrum*, Iran Journal of Radiation Research, 9(2), pp. 95-102, 2011.

[7] H. Tawara, K. Eda, T. Sanami, S. Sasaki, K. Takahashi, R. Sonkawade A. Nagamatsu, K. Kitajo, H. Kumagai, T. Doke, *Dosimetry for neutron from* 0.25 *to* 15 MeV *by the measurement of Linear Energy Distributions for secondary charged particles in CR-39 plastic*, Japanese Journal of Applied Physics, 47(3), p. 1726-1734, 2008.

[8] M. Caresana, M. Ferrarini, M. Fuerstner, S. Mayer, *Determination of LET in PADC detectors through the measurement of track parameters*, Nuclear Instruments and Methods in Physics Research A, 683, pp. 8–15, 2012.

[9] M. Caresana, M. Ferrarini, A. Parravicini, A. Sashala Naik, *Evaluation of a personal and environmental dosimetry with a dosimeter based on CR-39 SSNTD in quasi–monoenergetic neutron fields*, Radiation Protection Dosimetry, 161 (1–4), pp. 100–103, 2014.

[10] D. Nikezic, N. K. Yu, *Formation and growth of tracks in nuclear track materials*, Materials Science and Engineering, 46, pp. 51-123, 2004.

[11] International Commission on Radiological Protection (*ICRP*), *Conversion coefficients for use in radiological protection against external radiation*, *ICRP* Publication 74, Annals of *ICRP* 26 (3-4), 1996.

[12] A. Fassò, A. Ferrari, J. Ranft, P. R. Sala, *FLUKA: a multi–particle transport code*, Technical report *CERN*–2005–10, *INFN/TC*_05/11, *SLAC–R*–773, 2005.

[13] T. T. Böhlen, F. Cerutti, M. P. W. Chin, A. Fassò, A. Ferrari, P. G. Ortega, A. Mairani, P. R. Sala, G. Smirnov, V. Vlachoudis, *The FLUKA Code: Developments and Challenges for High Energy and Medical Applications*, Nuclear Data Sheets, 120, pp. 211-214, 2014.

[14] V. Gressier, J. F. Guerre-Chaley, V. Lacoste, L. Lebreton, G. Pelcot, J. L. Pochat, *AMANDE: a new facility for monoenergetic fields production between* 2 keV *and* 20 MeV, Radiation Protection Dosimetry, 110, pp. 49-52, 2010.

[15] Official site of the *IRSN-AMANDE* facility: < **https://www.irsn.fr/EN/Research/Scientific-tools/experimental-facilities-means/Amande/Pages/Amande-facility.aspx** > .

[16] M. Caresana, M. Ferrarini, A. Parravicini, *Analisi morfologica delle tracce nucleari su rivelatori CR-39*, Atti del Convegno Nazionale di Radioprotezione "Cinquantenario AIRP: Storia e Prospettive della Radioprotezione", Pisa, 2008.

[17] M. Bolzonella, M. Caresana, M. Ferrarini, *A self-consistent FLUKA algorithm for studying the response of passive dosimeters based on CR-39 track detectors in fast neutron fields*, Radiation Measurements, 138, 2020, 106456.

[18] R. L. Fleischer, P. B. Price, R. M. Walker, *Nuclear Tracks in Solids: Principles and Applications*, ch. 1–3, University of California Press, 1975.

[19] B. Dörschel, D. Hermsdorf, K. Kadner, S. Starke, *Dependence of the etch rate ratio on the energy loss of light ions in CR*-39, Radiation Measurements, 35, pp. 287-292, 2002.

[20] R. H. Olsher, T. D. McLean, A. L. Justus, R. T. Devine, M. S. Gadd, *Personal dose equivalent conversion coefficients for neutron fluence over the energy range of* 20–250 MeV, Radiation Protection Dosimetry, 138 (3), pp. 199-204, 2009.

[21] Y. Nakane, H. Nakashima, Y. Sakamoto, *Monte Carlo calculation and measurement of energy response of a solid state nuclear track detector to neutrons from* 100 keV *to* 20 MeV, Radiation Measurement, 27, pp. 445-452, 1997.

[22] International Organization for Standardization (*ISO*), *ISO 14146*, *Radiological protection – criteria and performance limits for the periodic evaluation dosimetry services*, *ISO*, 2018.